

**This item is the archived preprint of:**

Bottom-up sensory processing can decrease activity and functional connectivity in the default mode like network in rats

**Reference:**

Hinz Rukun, Peeters Lore, Shah Disha, Missault Stephan, Belloy Michaël, Vanreusel Verdi, Malekzadeh Meriam, Verhoye Marleen, Van Der Linden Anne-Marie, Keliris Georgios.- Bottom-up sensory processing can decrease activity and functional connectivity in the default mode like network in rats  
bioRxiv - ISSN 2692-8205 - 2018, p. 1-31

Full text (Publisher's DOI): <https://doi.org/10.1101/482638>

To cite this reference: <https://hdl.handle.net/10067/1710120151162165141>

1 **Bottom-up sensory processing can decrease**  
2 **activity and functional connectivity in the**  
3 **default mode like network in rats.**

4 *Rukun Hinz\**<sup>1</sup>, *Lore M. B. Peeters*<sup>1</sup>, *Disha Shah*<sup>1</sup>, *Stephan Missault*<sup>1</sup>, *Michaël Belloy*<sup>1</sup>, *Verdi*  
5 *Vanreusel*<sup>1</sup>, *Meriam Malekzadeh*<sup>1</sup>, *Marleen Verhoye*<sup>1</sup>, *Annemie Van der Linden*<sup>1</sup>, *Georgios A.*  
6 *Keliris*<sup>\*1</sup>

7 <sup>1</sup>Bio-Imaging Lab, University of Antwerp, Belgium

8  
9 **Keywords:** Resting state functional MRI, Functional connectivity, Visual stimulation, Default  
10 mode network, Rats

11  
12 **Journal aim:** Neuroimage

13  
14 **\*Corresponding authors**

15 Rukun Hinz  
16 Bio-imaging lab, University of Antwerp  
17 Campus Drie Eiken– Building Uc 1.17  
18 Universiteitsplein 1 -2610 Wilrijk – Belgium  
19 Tel. +3232652786  
20 Email: Rukun.Hinz@uantwerpen.be

21  
22 or

23  
24 Prof. Georgios Keliris  
25 Bio-imaging lab, University of Antwerp  
26 Campus Drie Eiken– Building Uc 1.07  
27 Universiteitsplein 1 -2610 Wilrijk – Belgium  
28 Tel. +32322652772  
29 Email: Georgios.Keliris@uantwerpen.be

30

31 **Abbreviations**

32	AC	Auditory cortex
33	BOLD	Blood oxygen level dependent
34	BVS	Blocked visual stimulation
35	Cg	Cingulate cortex
36	CVS	Continuous visual stimulation
37	DMLN	Default mode like-network
38	DMN	Default mode network
39	FC	Functional connectivity
40	fMRI	Functional magnetic resonance imaging
41	FOV	Field of view
42	FWE	Family wise error
43	GLM	General linear model
44	HRF	Hemodynamic response function
45	ICA	Independent component analysis
46	ISO	Isoflurane
47	LGN	Lateral geniculate nucleus
48	MD	Matrix dimensions
49	MED	Medetomidine
50	PtA	Parietal association cortex
51	ROI	Regions of interest
52	RS	Retrosplenial cortex
53	RSB	Resting state baseline scan
54	rsfMRI	Resting-state functional magnetic resonance imaging
55	RSNs	Resting state networks
56	SC	Superior colliculus
57	SS	Somatosensory cortex
58	ST	Slice thickness
59	TE	Echo time
60	TR	Repetition time
61	VC	Visual cortex

62 **Abstract**

63 The default mode network is a large-scale brain network that is active during rest and internally  
64 focused states and deactivates as well as desynchronizes during externally oriented (top-down)  
65 attention demanding cognitive tasks. However, it is not sufficiently understood if unpredicted  
66 salient stimuli, able to trigger bottom-up attentional processes, could also result in similar reduction  
67 of activity and functional connectivity in the DMN. In this study, we investigated whether bottom-  
68 up sensory processing could influence the default mode like network (DMLN) in rats. DMLN  
69 activity was examined using block-design visual functional magnetic resonance imaging (fMRI)  
70 while its synchronization was investigated by comparing functional connectivity during a resting  
71 versus a continuously stimulated brain state by unpredicted light flashes. We demonstrated that  
72 activity in DMLN regions was decreased during visual stimulus blocks and increased during  
73 blanks. Furthermore, decreased inter-network functional connectivity between the DMLN and  
74 visual networks as well as decreased intra-network functional connectivity within the DMLN was  
75 observed during the continuous visual stimulation. These results suggest that triggering of bottom-  
76 up attention mechanisms in anesthetized rats can lead to a cascade similar to top-down orienting  
77 of attention in humans and is able to deactivate and desynchronize the DMLN.

## 78 **1. Introduction**

79 The brain is a complex network consisting of functionally interconnected regions that dynamically  
80 communicate with each other. Part of these interactions can be observed non-invasively using  
81 resting-state functional magnetic resonance imaging (rsfMRI) (Damoiseaux et al., 2006; Salvador  
82 et al., 2005; van den Heuvel and Hulshoff Pol, 2010). This technique relies on the detection of low  
83 frequency fluctuations (0.01-0.2 Hz) in the blood oxygen level dependent (BOLD) signal while the  
84 subject is at rest, *i.e.* not performing any task. The coordinated fluctuations in the signals of  
85 anatomically separated regions have been shown to reflect intrinsic brain networks and evidence  
86 suggests that they correspond to spontaneous neuronal activity (Krishnan et al., 2018; Ma et al.,  
87 2016; Petridou et al., 2013). The regions that show temporally highly correlated activity are  
88 considered to be functionally connected and are referred to as resting state networks (RSNs)  
89 (Friston, 2011).

90 Since its discovery, rsfMRI has been widely used in human research to study RSNs in the healthy  
91 brain as well as their alterations in neuropathologies (Greicius, 2008; Hull et al., 2017; Zhou et al.,  
92 2017). More recently, comparable RSNs have also been detected in rodents (Gozzi and Schwarz,  
93 2016; Jonckers et al., 2011; C.P. Pawela et al., 2008; Sierakowiak et al., 2015). This finding has  
94 been very important as it opened a new window of pre-clinical investigations in (genetic) animal  
95 models of disease that can be investigated with different modalities at multiple scales, providing  
96 additional information about the underlying mechanisms (Nestler and Hyman, 2010; Trancikova  
97 et al., 2011). In addition, pre-clinical rsfMRI shows great potential in identifying early biomarkers  
98 for multiple neuropathologies and can be used as an excellent theranostic tool (Bertero et al., 2018;  
99 Li et al., 2017; Shah et al., 2016, 2013). However, the translation and interpretation of RSNs  
100 between rodents and humans remains challenging, among other reasons, due to the differences in  
101 anatomy, physiology and the required use of anesthesia in rodents (Pan et al., 2015). It is therefore

102 of utmost importance to investigate and improve our understanding of specific rodent RSNs that  
103 have been suggested to be homologous to RSNs in humans.

104 A RSN that has raised a lot of interest in humans is the default mode network (DMN), which has  
105 been shown to be most active during rest and internally focused tasks and less active during  
106 externally oriented attention demanding cognitive tasks (Greicius et al., 2003). Thus, it has been  
107 classified as a “task-negative network” and has been shown to alternate its activity with “task-  
108 positive networks” (Fox et al., 2005). The DMN is thought to play a fundamental role in self-  
109 referential thought, mind-wandering, internally-oriented cognition, and autobiographical memory  
110 (Lin et al., 2017). In humans, this network consists of regions in the anterior pre-frontal cortex,  
111 posterior cingulate cortex/retrosplenial cortex (precuneus), hippocampal formation, medial and  
112 lateral parietal regions (Buckner et al., 2008; Laird et al., 2009; Liska et al., 2015). A default mode  
113 like network (DMLN) suggested to be homologous to the human DMN has also been identified in  
114 rodents (Lu et al., 2012; Stafford et al., 2014). This DMLN comprises comparable regions, *i.e.*  
115 orbital cortex, prelimbic cortex, cingulate cortex, temporal association cortex, auditory cortex,  
116 posterior parietal cortex and parietal association cortex, retrosplenial cortex and hippocampus.  
117 Furthermore, besides anatomical similarities, few studies could indicate functional similarities such  
118 as the higher activity of the DMLN during rest vs task and the anti-correlation relationship of the  
119 DMLN with the task positive network (Rohleder et al., 2016; Schwarz et al., 2013).

120 In recent years, multiple human studies have shown that functional connectivity (FC) within the  
121 DMN is decreased when subjects are in a higher attentive and cognitive brain state associated with  
122 performing an internally guided (top-down) attention-demanding task (Elton and Gao, 2015;  
123 Fransson, 2006; Gao et al., 2013; Marrelec and Fransson, 2011). It is thought that this internally  
124 guided attention to external sensory input can suppress other internal processes associated with the  
125 DMN, resulting in this network’s inactivation and relative disconnection (Gao et al., 2013; Mayer

126 et al., 2010). However, it is not yet sufficiently understood if attentional guidance by externally  
127 driven factors (bottom-up) could also result in similar reduction of activity and connectivity in the  
128 DMN. In humans, some studies suggested that the DMN is not deactivated by simple sensory  
129 processing (Greicius et al., 2003). It should be noted, however, that the stimulus design in these  
130 studies was simple and predictable and thus not expected to continuously drive bottom-up attention.  
131 Interestingly, a study using simple but unpredictable visual stimuli could dynamically activate  
132 attention network and DMN indicating their interaction during stimulus-driven processes of  
133 attention (Hahn et al., 2007).

134 Neurophysiological experiments in the past few years suggest that top-down and bottom-up  
135 processes share overlapping neural systems and in particular the employment of the prefrontal and  
136 parietal network (for a review see (Katsuki and Constantinidis, 2014)). We conjectured, that  
137 similarly to top-down, bottom-up attention triggering stimuli could also deactivate DMN and  
138 reduce its connectivity. To test this hypothesis, we performed fMRI experiments in anesthetized  
139 rats driven by randomized (unpredictable) continuous visual stimulation (CVS) and compared  
140 DMLN activity and connectivity with a resting state baseline scan (RSB) and a blocked visual  
141 stimulation (BVS) design.

## 142 **2. Material and Methods**

### 143 **2.1. Animals and ethical statement**

144 In this study, we used male Long Evans wild type rats (N=12) of 4 months of age (Long Evans,  
145 Janvier). Rats were kept under a normal day/night cycle (12/12) with an average room temperature  
146 of 20-24°C and 40% humidity. Furthermore, rats were group housed and had *ad libitum* access to  
147 standard rodent chow and water. One animal was excluded from the analysis due to the detection  
148 of unilateral ventricular enlargement. All procedures were performed in accordance with the  
149 European Directive 2010/63/EU on the protection of animals used for scientific purposes. The

150 protocols were approved by the Committee on Animal Care and Use at the University of Antwerp,  
151 Belgium (permit number: 2015-50), and all efforts were made to minimize animal suffering.

## 152 **2.2. Animal preparation and anesthesia**

153 Rats were first anesthetized using 5% isoflurane for induction and 2% isoflurane for maintenance  
154 (IsoFlo, Abbott Illinois, USA) in a mixture of 70% N<sub>2</sub> and 30% O<sub>2</sub>. Animals were head fixed in  
155 the scanner using bite- and ear-bars and ophthalmic ointment was applied to the eyes. As soon as  
156 the animal was fixed in the scanner, medetomidine anesthesia (Domitor, Pfizer, Karlsruhe,  
157 Germany) was administered via a subcutaneous bolus of 0.05 mg/kg and isoflurane concentration  
158 was decreased to 0% over a time period of 5 minutes. Continuous subcutaneous infusion of  
159 medetomidine anesthesia of 0.1 mg/kg.h was started 15 minutes post bolus injection. Functional  
160 MRI scans were acquired starting from 30 min post-bolus injection until 1h05 min post bolus  
161 injection. The physiological status of the animals was monitored throughout the entire imaging  
162 procedure. Respiratory rate was obtained from a pressure sensitive pad (MR-compatible Small  
163 Animal Monitoring and Gating system, SA Instruments, Inc.) with a sampling rate of 225 Hz. Body  
164 temperature was closely monitored using a rectal thermistor and was maintained between (37.0 ±  
165 0.1 °C) using a feed-back controlled warm air heat system (MR-compatible Small Animal Heating  
166 System, SA Instruments, Inc.). Furthermore, blood oxygenation was recorded using a pulse  
167 oxygenation meter (MR-compatible Small Animal Monitoring and Gating system, SA Instruments,  
168 Inc. ) with a sampling rate of 450 Hz. After imaging procedures, animals received a subcutaneous  
169 bolus injection of 0.1 mg/kg atipamezole (Antisedan, Pfizer, Karlsruhe, Germany) to counteract  
170 the effects of medetomidine and were placed in a recovery box with infrared heating for post-scan  
171 monitoring until the animal was fully awake.

## 172 **2.3. MRI**



173 All imaging procedures were performed with Paravision 6.0 using a 9.4 T BioSpec MR system  
174 (Bruker, Germany) with an active decoupled rat quadrature surface coil (Rapid biomedical,  
175 Germany) and a 98 mm diameter quadrature volume resonator for transmission (Bruker, Germany).  
176 First, three orthogonal anatomical multi-slice Turbo RARE T2-weighted images (field of view  
177 (FOV): (30x30) mm<sup>2</sup>, matrix dimensions (MD): [256x256], 12 slices, Slice thickness (ST): 0.9  
178 mm, echo time (TE)/ repetition time (TR): 33/2500 ms, RARE factor: 8) were acquired to allow  
179 reproducible flat skull positioning of coronal slices. Then, a coronal anatomical reference scan was  
180 acquired using a multi-slice Turbo RARE T2-weighted sequence (FOV: (30x30) mm<sup>2</sup>, MD:  
181 [256x256], 12 slices, ST: 0.9 mm, TE/TR: 33/2500 ms, RARE factor: 8), covering the brain from  
182 3.3 mm anterior to bregma to 7.5 mm posterior to bregma (suppl. figure 1). Next, a B<sub>0</sub> field map  
183 was acquired to assess field homogeneity, followed by local shimming in a rectangular volume of  
184 interest in the brain to correct for the measured inhomogeneities. The RSB scan had an identical  
185 geometry to the reference scan and was acquired using a T2\*-weighted single shot echo planar  
186 imaging (EPI) sequence (FOV: (30x30) mm<sup>2</sup>, MD: [128x98], 12 slices, ST: 0.9 mm, TE/TR:  
187 18/2000 ms) resulting in a voxel dimension of (0.234 x 0.313 x 0.9) mm<sup>3</sup> and a total scan duration  
188 of 10 min (300 volumes). Subsequently, random continuous light flickering (see section 2.4) was  
189 turned on and after 1 minute the CVS scan was acquired using the same parameters as the RSB  
190 (300 volumes). Last, a BVS data set was acquired using the same parameters and sequence (380  
191 volumes; Figure 1A).

## 192 **2.4. Visual stimulation**

193 Visual stimulation with flickering light was presented using a white LED coupled to a fiber-optic  
194 cable, which was centrally placed in front of the animal's head. The LED light was controlled by  
195 a voltage-gated device to control the triggering of the LED light (ON-OFF) driven by a RZ2  
196 BioAmp Processor (Tucker-Davis, Alachua). Stimulus timing and alignment to the MR imaging

197 was achieved by TTL pulses sent by the scanner at the beginning of every volume of the fMRI  
198 scan.

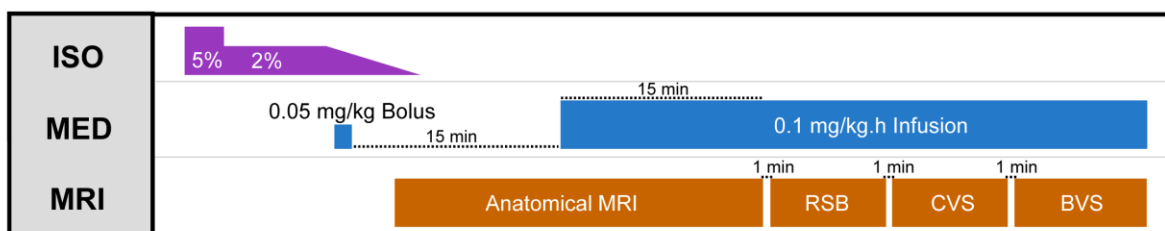
#### 199 2.4.1. Continuous visual stimulation

200 The CVS was used to induce a continuous visual sensory drive with randomization of light pulses  
201 to avoid sensory adaptation effects and to constantly trigger bottom-up attention mechanisms. This  
202 condition can be assumed to create a steady brain state similar to rest and thus could be analyzed  
203 the same way as the RSB scan (Figure 1B-D). The CVS was initiated 1 min before the start of the  
204 acquisition to avoid the detection of the initial transient increase of brain activity, which occurs  
205 when the visual stimulation is turned on. The stimulation paradigm was controlled via Matlab code  
206 (MATLAB R2014a, The MathWorks Inc. Natick, MA, USA) using an USB to serial port  
207 connection (IC-232A, Rotronic) and consisted of continuous short pulses of light and inter-light  
208 intervals (both with a random duration between 50-250 ms) (Figure 1B). Convolution of the CVS  
209 stimulus paradigm with the canonical hemodynamic response function (HRF) in SPM12 was  
210 performed in order to demonstrate that the expected signal fluctuations from CVS are negligible in  
211 comparison to those expected by the BVS paradigm (Figure 1C).

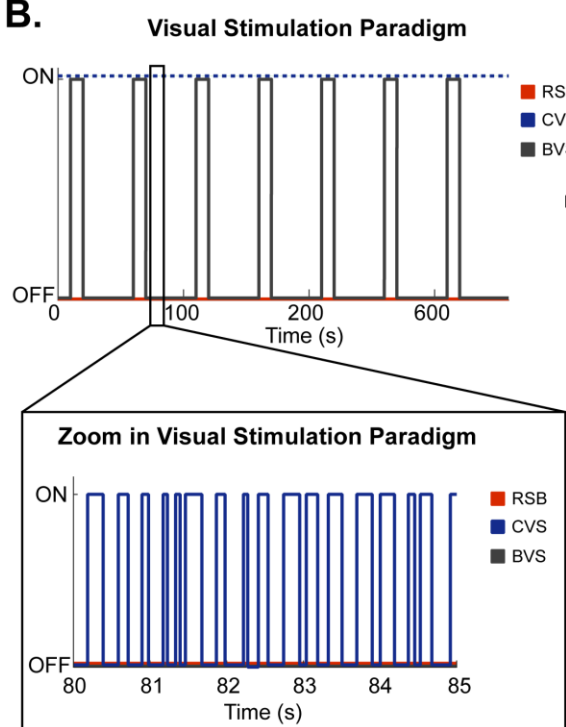
#### 212 2.4.2. Block design visual stimulation

213 To evoke BOLD responses from the visual system, fMRI scan was acquired during a block design  
214 paradigm with a visual stimulation frequency of 4 Hz, duty cycle 50% (125 ms ON/OFF), an initial  
215 OFF block of 10 seconds followed by 15 ON/OFF blocks of 10 s and 40 s respectively (Figure 1B-  
216 C).

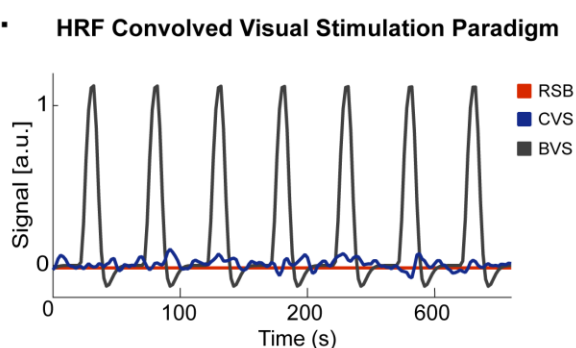
A.



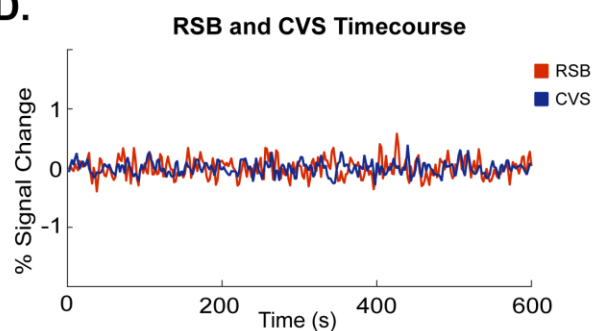
B.



C.



D.



217

218

219

220

221

222

223

224

225

226

**Figure 1. Scanning protocol and visual stimulation paradigms.** A. Scanning protocol. For handling procedures, animals were first anesthetized using 5% isoflurane (ISO) for induction followed by 2% ISO for maintenance. Once the animal is fixated in the scanner bed, a bolus of 0.05mg/kg of medetomidine (MED) was administered and ISO anesthesia was gradually decreased to 0% ISO. After 15 minutes post bolus injection, a continuous infusion of 0.1 mg/kg.h MED was administered to the animal. For imaging procedures, first a set of anatomical Turbo RARE T2 scans were acquired and shimming procedures were performed. Next, 30 min post bolus injection a resting state baseline (RSB) scan was acquired. Subsequently, continuous visual stimulation (CVS) paradigm was turned on and after one

227 *minute the CVS scan was acquired. Lastly, after a recovery time of 1 minute a block design*  
228 *visual stimulation (BVS) fMRI scan was acquired. B. Visual stimulation paradigm of RSB, CVS*  
229 *and BVS scan indicating when visual stimuli was turned on or off. C. Haemodynamic Response*  
230 *Function (HRF) convolved visual stimulation paradigm of RSB, CVS and BVS scan showing*  
231 *predicted BOLD signal response in arbitrary units (a.u.) from each condition. D. Example of*  
232 *acquired RSB and CVS normalized BOLD signal time course in the visual network.*

### 233 **2.5. Breathing rate processing**

234 Breathing rate pressure signals were analyzed to investigate the potential influence of visual  
235 stimulation on the animals' physiology. First, breathing rates were calculated for each volume by  
236 calculating the median period of the breathing cycle between the initial and the following volume  
237 and inverting this value to breaths per minute. For resting state data, averaged breathing rate from  
238 the complete scans were compared between the RSB and CVS condition using a paired t-test  
239 ( $p < 0.05$ ). For the BVS scans, averaged breathing rate over all visual stimulation blocks was  
240 compared ten seconds before with ten seconds during visual stimuli using a paired t-test.

### 241 **2.6. MRI Processing**

242 All data processing was performed using SPM 12 software (Statistical Parametric Mapping,  
243 <http://www.fil.ion.ucl.ac.uk>), REST toolbox (REST1.7, <http://resting-fmri.sourceforge.net>) and  
244 GIFT toolbox (Group ICA of fMRI toolbox version 3.0a: <http://icatb.sourceforge.net/>).  
245 Pre-processing consisted of realignment of the data towards the first image of each scan using a 6-  
246 parameter (rigid body) spatial transformation, normalization towards a study specific EPI template  
247 using a global 12-parameter affine transformation, followed by a non-linear transformation.  
248 Finally, data were smoothed in-plane using a Gaussian kernel with a full width at half maximum  
249 of twice the voxel size (0.458 x 0.626 mm). rsfMRI data were then further band pass filtered  
250 between 0.01-0.2 Hz using REST toolbox.

251           2.6.1. Functional connectivity

252                   2.6.1.1. ICA components

253 To obtain the RSNs from the rsfMRI data, an independent component analysis (ICA) was  
254 performed on RSB data. First, movement was regressed out of the data based on the estimators  
255 from the realignment procedure using the REST toolbox. Next, ICA was performed in GIFT using  
256 the Infomax algorithm with predefined number of 15 components as used previously (Jonckers et  
257 al., 2011). Components representing functional networks were identified by comparison to  
258 previous observed RSNs and discarding a minority of artefactual components (e.g. only edge of  
259 the brain) by careful visual inspection (Gozzi and Schwarz, 2016; Jonckers et al., 2011; Lu et al.,  
260 2012; C.P. Pawela et al., 2008; Sierakowiak et al., 2015). Afterwards, the selected mean z-scored  
261 RSNs group components were thresholded at z-score > 1 to obtain a mask of each network.

262                   2.6.1.2. ICA-based inter-network connectivity

263 To evaluate inter-network connectivity, network masks were used as regions of interest (ROI) in  
264 correlation-based analysis per subject. Pairwise Pearson correlation coefficients between the  
265 average BOLD time series of each network ROI were calculated and Fisher z-transformed using  
266 an in-house Matlab program. Mean Fisher z-transformed inter-network correlation matrices were  
267 calculated for RSB and CVS conditions. Statistical analysis between conditions was performed  
268 using a repeated measures 2-way ANOVA ( $p < 0.05$ , Sidak correction for multiple comparisons).  
269 To calculate the FC between the DMLN and visual network, z-transformed correlation values of  
270 the cingulate-retrosplenial, hippocampal and temporal-prefrontal with visual network were  
271 averaged. Differences in correlation between the two conditions were then investigated using  
272 pairwise t-test ( $p < 0.05$ ).

273                   2.6.1.3. ROI-based intra- and inter-network connectivity

274 To investigate within and between network connectivity differences, specific anatomically defined  
275 bilateral ROIs were selected in the DMLN (based upon the RSB ICA networks: cingulate cortex  
276 (Cg), retrosplenial cortex (RS), parietal association cortex (PtA), temporal association cortex  
277 (TeA)) as well as in the visual system (based upon the visual stimulation correlated ICA component  
278 of the BVS: lateral geniculate nucleus (LGN), superior colliculus (SC), visual cortex (VC)) (suppl.  
279 figure 2). Furthermore, a ROI in the primary somatosensory cortex (SS) was added as a control  
280 region. Pairwise Pearson correlation coefficients between the average BOLD time series of each  
281 ROI were calculated and Fisher z-transformed. Mean z-transformed ROI connectivity matrices  
282 were calculated for RSB and CVS conditions. To compare RSB and CVS condition, statistical  
283 analysis between conditions was performed using a repeated measures 2-way ANOVA ( $p < 0.05$ ,  
284 Sidak correction for multiple comparisons).

#### 285 2.6.1.4. Seed-based analysis

286 To investigate how the full-brain FC of the Cg is influenced by CVS, seed-based analysis was  
287 performed. To this end, the mean time course of Cg was used as a predictor in a General linear  
288 model (GLM) and motion parameters were included as covariates. Each subject's FC between Cg  
289 and DMLN or visual network was extracted by using the respective binarized masks derived from  
290 the ICA and calculating the mean T-values within this mask for each individual subject. The  
291 DMLN network mask was constructed by the union of the cingulate-retrosplenial network mask,  
292 hippocampal network mask and temporal-prefrontal network mask. Statistical analysis to compare  
293 differences between the conditions was performed by means of a paired t-test ( $p < 0.05$ ).

#### 294 2.6.2. Block design fMRI

295 BVS data were processed using a group ICA approach using the GIFT toolbox with an Infomax  
296 algorithm and 15 predefined components. Group ICA analysis was chosen instead of the standard  
297 GLM to increase sensitivity towards detecting responding brain regions by not relying on

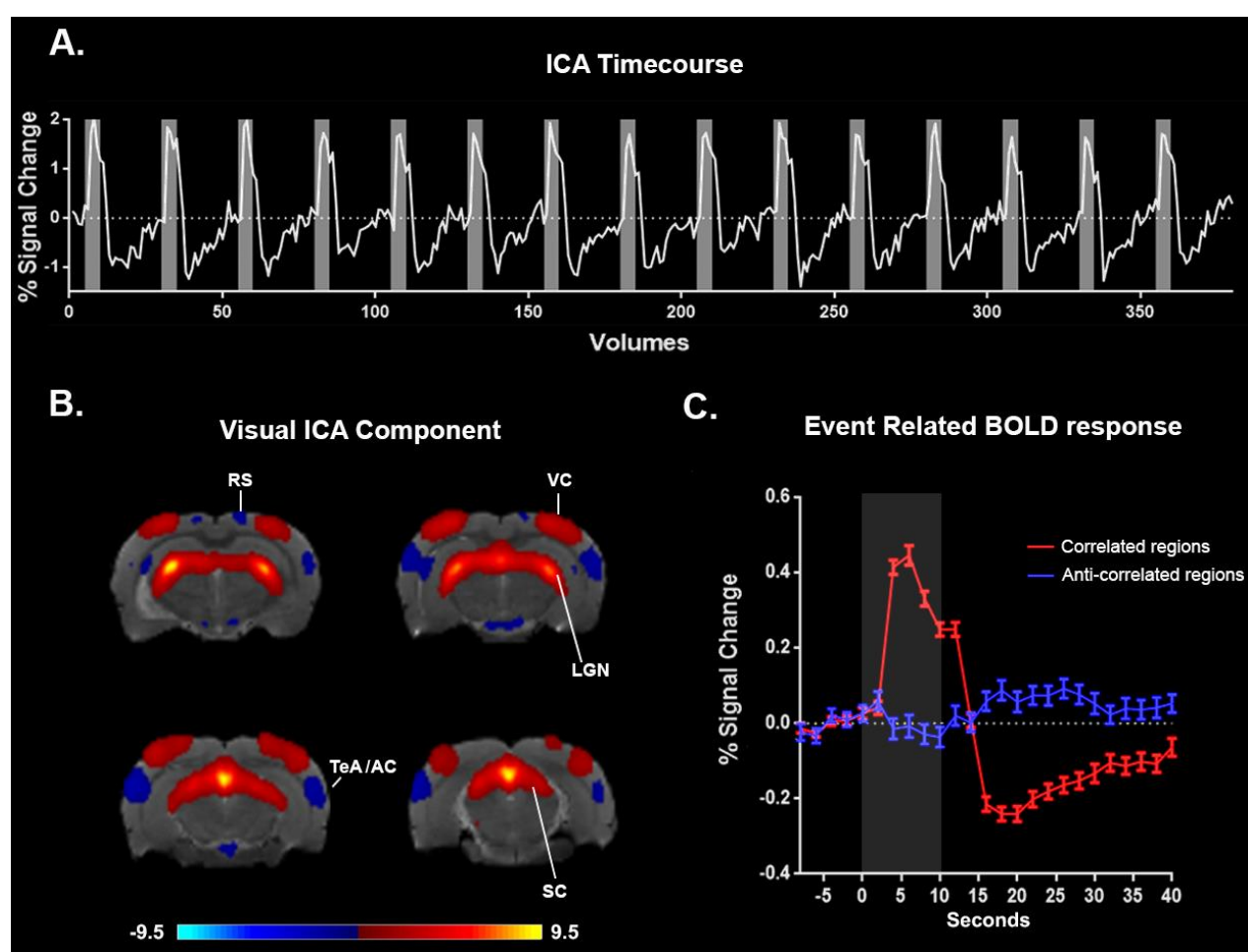
298 predetermined BOLD HRF functions (Calhoun et al., 2009). The components temporal correlation  
299 with the visual stimulation paradigm was then calculated using R-square statistic in the GIFT  
300 toolbox. The component with highest temporal correlation with the visual stimulation paradigm  
301 were regarded as responding regions. Event related BOLD responses were extracted from a binary  
302 mask of responding regions, which are either correlated ( $z$ -score  $> 1$ ) or anti-correlated ( $z$ -score  $<$   
303  $-1$ ) with the ICA time course. To confirm our results, GLM analysis was performed for each subject  
304 within the ICA component mask ( $z$ -score  $> 1$  and  $< -1$ ) of the responding regions using a canonical  
305 HRF function in SPM 12. The model was set to either detect a positive BOLD response during the  
306 stimulation period, to locate visual responding regions, or during the rest period, to detect regions  
307 which are more active during rest vs stimulation period i.e. DMLN activity. One sample t-test  
308 ( $p < 0.001$ , uncorrected for multiple comparisons) was performed to evaluate BSV group response.

### 309 **3. Results**

#### 310 **3.1. Block-design visual stimulation**

311 To investigate whether activity in the DMLN of anesthetized rats is changing between visual  
312 sensory stimulation and rest periods, we analyzed the block-design fMRI experiment. To this end,  
313 we performed group-ICA analysis and sorted the components based on their temporal correlation  
314 with the visual stimulation paradigm. The component with the highest correlation ( $R^2=0.64$ )  
315 showed clear BOLD signal increases during the ON-blocks indicating a strong visual activation of  
316 multiple responding regions (Figure 3A). The mean group statistical ICA map ( $z$ -score  $> 1$  and  $<$   
317  $-1$ ) of this component revealed that the activated regions were, as expected, areas involved in visual  
318 processing, *i.e.* the LGN, SC, VC (Figure 3B). Event related analysis of all regions which are  
319 correlated with the ICA time course demonstrated that visual stimulation evoked a positive BOLD  
320 response as expected (Figure 3C). Interestingly, we also observed regions such as the temporal  
321 association cortex/auditory cortex (TeA/AC) and RS, being anti-correlated to the ICA component's

322 time course, indicating higher BOLD signal during rest vs stimulation (Figure 3B). Event related  
323 analysis of anti-correlated regions with the ICA time course showed a subtle BOLD signal decrease  
324 during visual stimulation which rebounded and increased during blanks (Figure 3C). To confirm  
325 our results, GLM modeling was applied and detected increased BOLD response during visual  
326 stimulation in LGN, SC and VC as well as increased BOLD response during blanks in TeA/AC  
327 (suppl. figure 3).  
328



329  
330 **Figure 3. Functional MRI ICA.** A. ICA Time course. Time course from mean group visual ICA  
331 component with highest temporal correlation ( $R^2=0.64$ ) with the visual stimulation paradigm (grey  
332 blocks). B. Visual ICA Component. Mean statistical group ICA map ( $z$ -score  $-1 < \text{and} > 1$ )



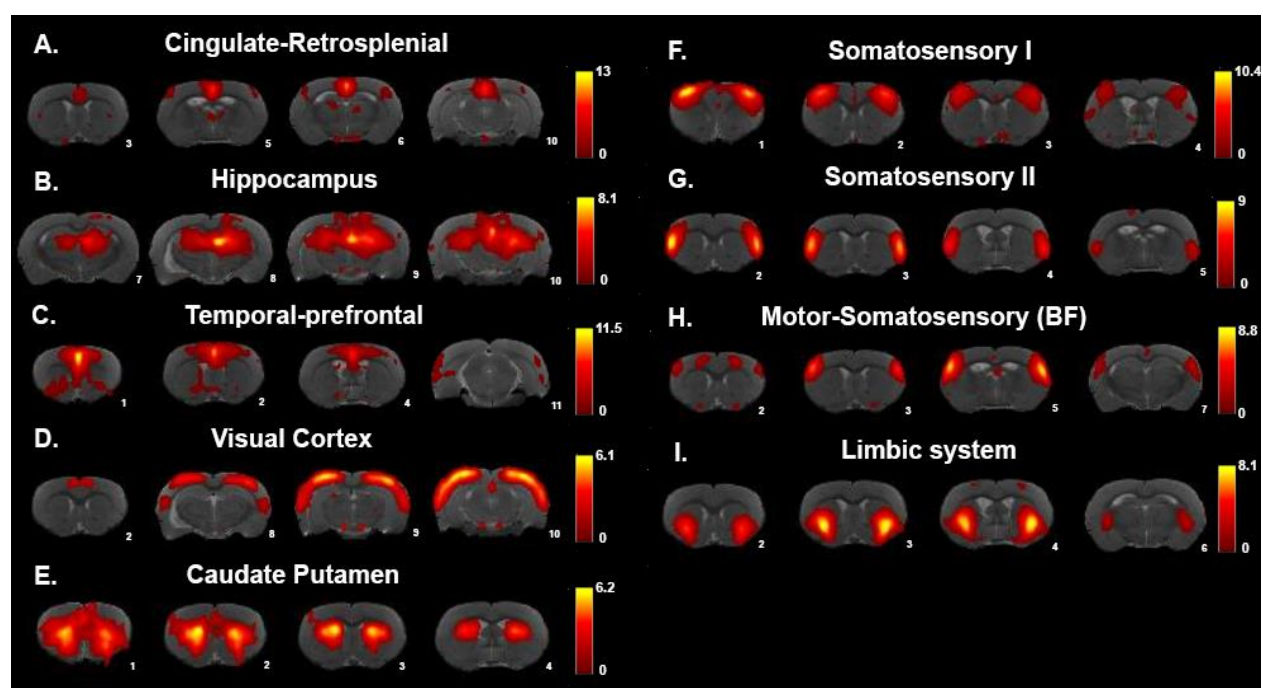
333 *demonstrating areas which are correlated to the mean ICA component's time course involved in*  
334 *visual processing, i.e. visual cortex (VC), lateral geniculate nucleus (LGN) and superior colliculus*  
335 *(SC). Regions demonstrating a BOLD time course that is anti-correlated with the mean ICA*  
336 *component's time course, meaning higher BOLD signal during rest than during visual stimulation,*  
337 *were observed in DMLN regions i.e. temporal association cortex/auditory cortex (TeA/AC) and*  
338 *retrosplenial cortex (RS). C. Event related response of the regions correlating (Red) and anti-*  
339 *correlating (Blue) to the ICA component's time course. Grey block indicates visual stimulation*  
340 *period*

### 341 **3.2. Resting state vs Continuous Visual Stimulation**

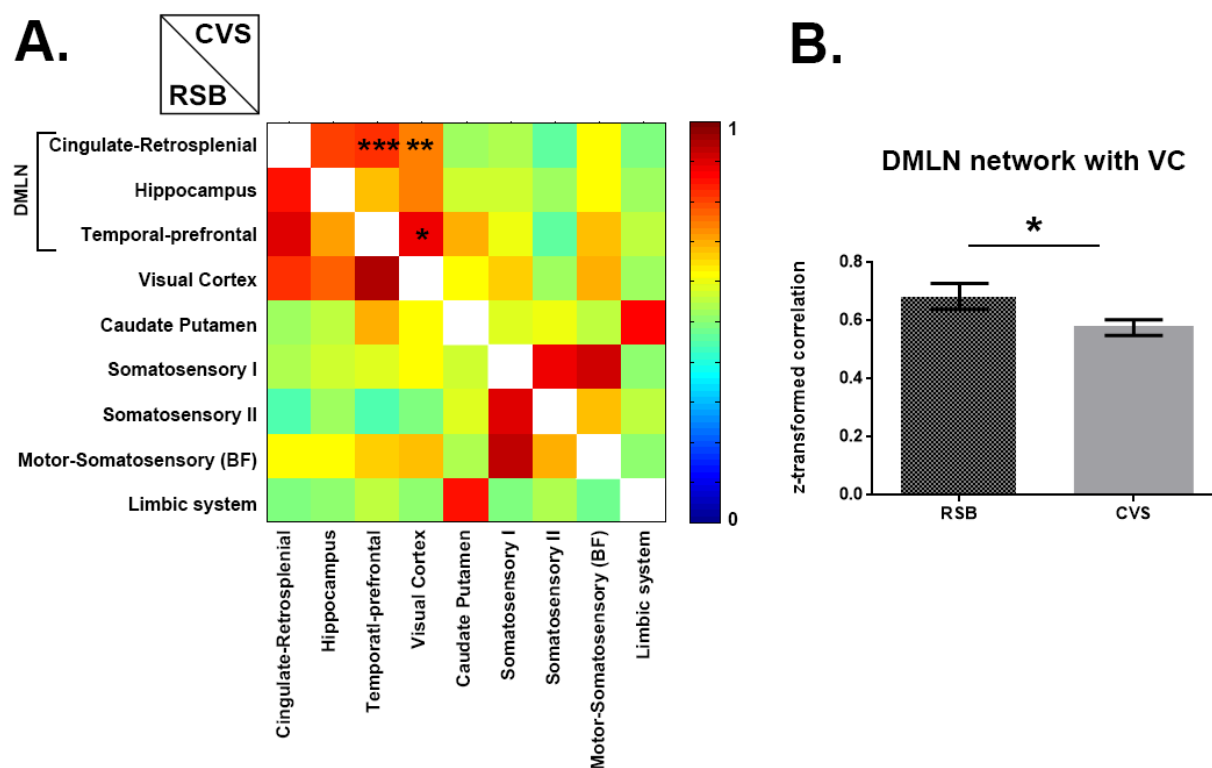
#### 342 **3.2.1. Decreased intra- and inter-network connectivity during CVS**

343 To identify potential changes in FC induced by our randomized continuous stimulation paradigm,  
344 we first performed group-ICA for the RSB condition and identified commonly observed RSNs.  
345 Functionally relevant components included three subnetworks of the DMLN: a cingulate-  
346 retrosplenial network (with cingulate cortex, retrosplenial cortex and parietal association cortex),  
347 a hippocampal network (with subiculum, dentate gyrus, CA1 and CA3), and a temporal-prefrontal  
348 network (with orbito-frontal cortex, prelimbic cortex and temporal association cortex).  
349 Furthermore, ICA analysis detected a visual network, a caudate putamen network, a primary and  
350 secondary somatosensory network, a barrel field network and a limbic network (including the  
351 amygdala and ventral striatum). Next, to evaluate intra- and inter-network connectivity, we  
352 threshold each ICA-component map ( $z$ -values  $> 1$ ), extracted the time-courses and performed  
353 pairwise correlations for both the RSB and CVS conditions (Figure 5). Statistical analysis  
354 comparing RSB and CVS condition using a repeated measures 2-way ANOVA (multiple  
355 comparison correction Sidak  $p < 0.05$ ) detected a significantly decreased intra-DMLN network  
356 correlation in the CVS condition (*i.e.* subnetworks cingulate-retrosplenial and temporal-prefrontal

357 ( $p < 0.001$ ) as well as decreased inter-network correlations between DMLN subnetworks and the  
358 visual network (*i.e.* cingulate-retrosplenial network with visual network ( $p = 0.002$ ) and temporal-  
359 prefrontal network with visual network ( $p = 0.027$ ).



360  
361 **Figure 4. ICA of Resting State Baseline (RSB) condition.** Mean group statistical ICA maps ( $z$ -  
362  $score > 1$ ) revealed nine functionally relevant components. A.-C. The DMLN in rats split up in three  
363 subcomponents *i.e.* A. Cingulate-Retrosplenial Network (with cingulate, retrosplenial cortex and  
364 parietal association cortex), B. Hippocampal network (with subiculum, dentate gyrus, CA1 and  
365 CA3) and C. Temporal-prefrontal network (with orbito-frontal cortex, prelimbic cortex and  
366 temporal association cortex). D. Visual network (with visual and somatosensory cortex). E.  
367 Caudate Putamen network. F.-G. Primary and secondary somatosensory network. H. Barrel field  
368 network. I. Limbic network (with amygdala and ventral striatum).

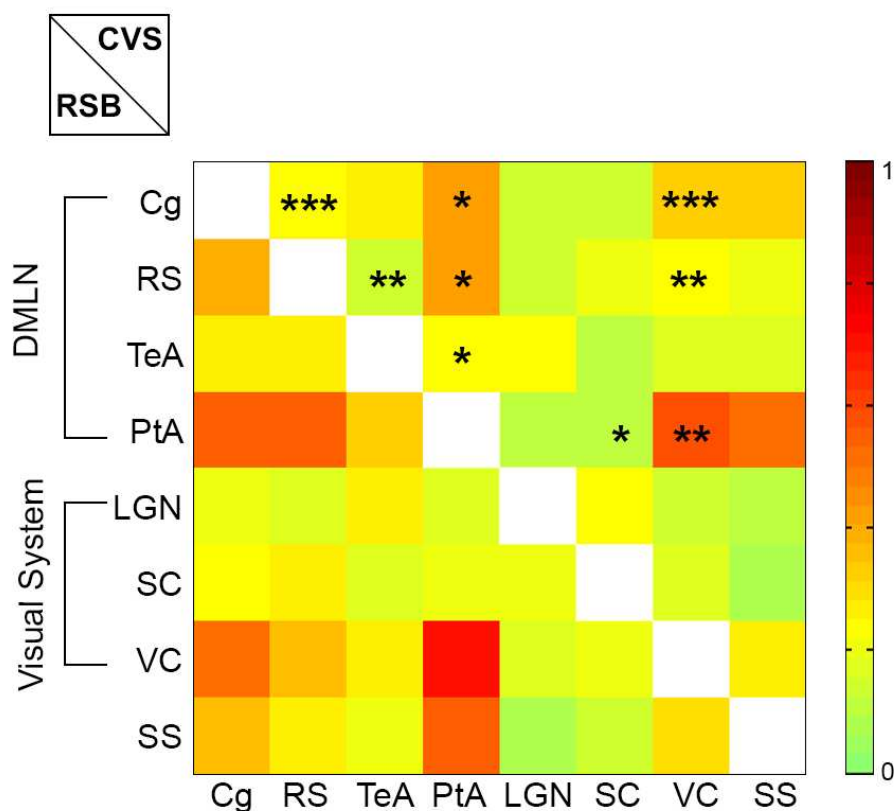


369  
 370 **Figure 5. Inter-network functional connectivity.** A. Pairwise z-transformed Pearson correlation  
 371 matrix of network components' time courses of the resting state baseline (RSB) (Bottom) and of the  
 372 continuous visual stimulation (CVS) condition (Top). Stars indicate significant differences found  
 373 between the two conditions with repeated measures 2-way ANOVA ( $p < 0.05$ , with Sidak multiple  
 374 comparison correction). For CVS, significant decreased inter-network connectivity was found  
 375 between subnetworks of the DMLN (i.e. cingulate-retrosplenial network and temporal-prefrontal  
 376 network) and between DMLN subnetworks and visual network. Color bar represents z-values.  
 377  $*p < 0.05$ ,  $**p < 0.005$ ,  $***p < 0.001$  B. Inter-network connectivity between DMLN and Visual  
 378 network (average of connectivity between cingulate-retrosplenial network and visual network,  
 379 hippocampal network and visual network, and temporal-prefrontal network and visual network).  
 380 Statistical analysis using a paired t-test detected a significant decreased inter-network connectivity  
 381 in the CVS condition as compared to the RSB condition ( $p < 0.05$ ).  
 382

383 Since CVS induced decreased inter-network correlation between the DMLN subnetworks and the  
384 visual network, we further assessed the pairwise correlation between specific ROIs of these  
385 networks to zoom-in and better understand the sources of these decreases. ROIs in DMLN (*i.e.* Cg,  
386 RS, TeA and PtA) and visual system (*i.e.* LGN, SC and VC) were selected. In addition, we included  
387 the SS as a control area. Pairwise correlation between each ROI's averaged BOLD time course was  
388 performed and compared between RSB and CVS condition (Figure 6). Statistical analysis using a  
389 repeated measures 2-way ANOVA (Sidak multiple comparisons correction  $p < 0.05$ ) showed a  
390 decreased correlation between the DMLN ROIs *i.e.* Cg-RS ( $p < 0.001$ ), Cg-PtA ( $p = 0.005$ ), RS-TeA  
391 ( $p = 0.002$ ) and RS-PtA ( $p = 0.006$ ) as well as between DMLN and visual ROIs *i.e.* Cg-VC ( $p < 0.001$ ),  
392 RS-VC ( $p = 0.005$ ), PtA-SC ( $p = 0.036$ ), and PtA-VC ( $p = 0.002$ ). None of these areas showed a  
393 significant change in correlation with the SS.

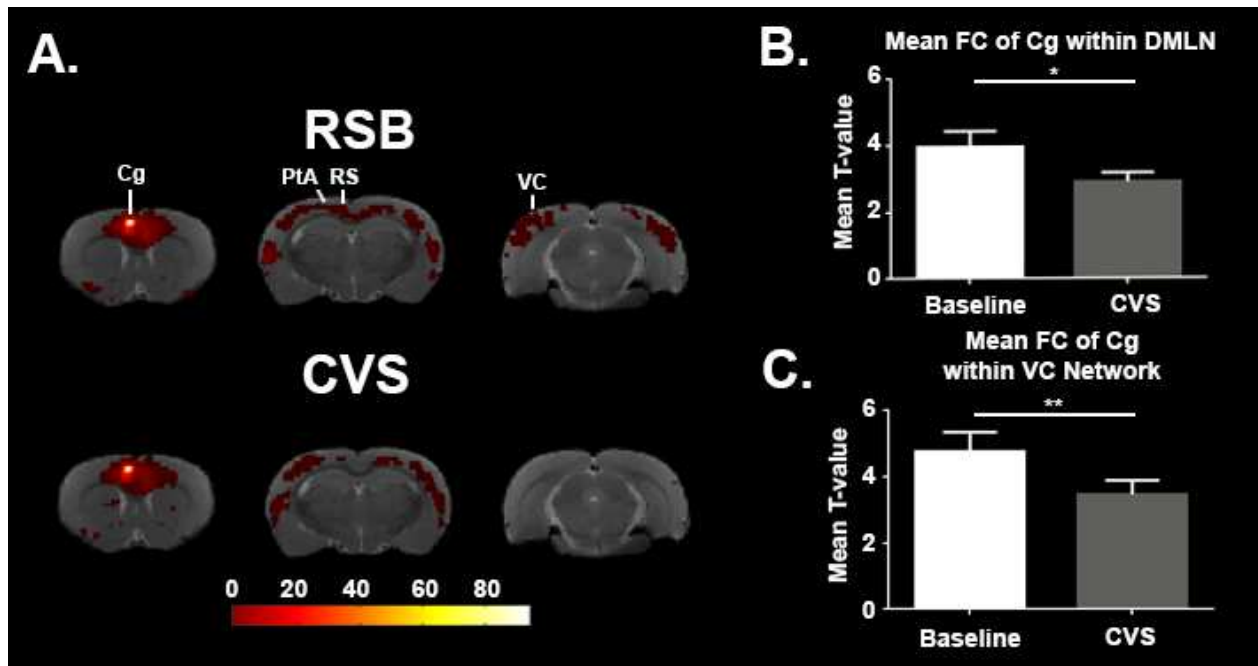
### 394 **3.2.2. Voxel-based functional connectivity of Cingulate cortex**

395 The cingulate cortex, a major node of both DMLN in rodents as well as DMN in humans has been  
396 shown to change its activity during unpredictable stimuli (Hahn et al., 2007). Since our stimuli in  
397 the CVS condition were similarly designed to be unpredictable we selected this area for seed-based  
398 analysis. As demonstrated in the statistical FC maps (one sample t-test,  $p < 0.001$ , family wise error  
399 (FWE) corrected for multiple comparisons) presented in Figure 7A, the Cg demonstrated wider  
400 brain connectivity during the RSB in comparison to the CVS condition. To further quantify this  
401 effect, we performed a paired t-test for the T-values within the DMLN or visual network. We found  
402 that CVS condition induced a decreased correlation between Cg and DMLN as well as between Cg  
403 and the visual network (Figure 7B-C).



404  
 405 **Figure 6. ROI based analysis.** A. Pairwise z-scored Pearson functional connectivity (FC) matrix  
 406 between time courses of ROIs of the DMLN (i.e. cingulate cortex (Cg), retrosplenial cortex (RS),  
 407 temporal association cortex (TeA) and parietal association cortex (PtA)), the visual system (i.e.  
 408 lateral geniculate nucleus (LGN), superior colliculus (SC) and visual cortex (VC)) and the  
 409 somatosensory cortex (SS) as a control region. Top half of the matrix represents FC of continuous  
 410 visual stimulation (CVS) condition. Bottom half of the matrix represents FC of resting state  
 411 baseline (RSB) condition. Color bar represents z-values. Stars indicate significant differences  
 412 found between the two conditions (diagonally symmetric positions) with repeated measures 2-way  
 413 ANOVA ( $p < 0.05$ , with Sidak multiple comparison correction). Decreased FC was detected  
 414 between DMLN ROIs i.e. Cg-RS, Cg-PtA, RS-TeA and RS-PtA as well as between DMLN and visual  
 415 system ROIs i.e. Cg-VC, RS-VC, Pta-SC and PtA-VC. \* $p < 0.05$ , \*\* $p < 0.005$ , \*\*\* $p < 0.001$

416



417

418 **Figure 7. Seed based analysis of functional connectivity with the cingulate cortex as seed region.**

419 *A. Statistical maps of functional connectivity ( $p < 0.05$  with family wise error correction (FWE) for*

420 *multiple comparison correction) of the cingulate cortex (Cg) in the resting state baseline (RSB)*

421 *condition (Top) and continuous visual stimulation (CVS) condition (Bottom). Decreased FC in the*

422 *parietal association cortex (PtA), retrosplenial cortex (RS- and visual cortex (VC) was observed*

423 *in the CVS condition. Color bar represents t-values. High t-values indicate high functional*

424 *connectivity with the seed B. Bar graph of the mean T-value with  $\pm$  SEM within the default mode*

425 *like network. For each subject, mean T-values were extracted within the default mode like network*

426 *ICA mask. Results show that CVS significantly decreased connectivity of the Cg (paired t-test,*

427  *$p < 0.05$ ) with the default mode like network. C. Bar graph of the Mean T-value with  $\pm$  SEM of all*

428 *subjects within the Visual network (VC). For each subject, mean T-values were extracted within*

429 *the VC network ICA mask. Results show that continuous visual stimulation (CVS) significantly*

430 *decreased connectivity of the Cg (paired t-test,  $p < 0.05$ ) with the VC network.*

### 431 **3.3. Unaltered breathing rate during visual stimulation**

432 The pressure signal for breathing rate of the animals was recorded throughout the whole experiment  
433 and analyzed to assess potential changes on the general physiological state due to the visual  
434 stimulation. A paired t-test showed that there were no significant changes in breathing rate due to  
435 the visual stimulation ( $p=0.79$ ) (suppl. figure 4A). Breathing rate was further compared between  
436 RSB and CVS conditions using a paired t-test ( $p<0.05$ ). Likewise, CVS did not significantly alter  
437 the breathing rate ( $p=0.1$ ) (suppl. figure 4B).

## 438 **4. Discussion**

439 In the current study, we investigated the impact of visual stimulation on the DMLN activity and its  
440 FC in rats. We found that visual stimulation could deactivate nodes of the DMLN and could  
441 decrease FC within DMLN as well as across DMLN and visual networks.

### 442 **4.1. Block design visual stimulation induces deactivation in DMLN regions**

443 Block design visual stimulation was performed a) to identify the visually responsive areas and b)  
444 to investigate the influence of visual stimulation on the DMLN.

445 Similar to previous visual fMRI studies in rats, we detected activation of visual processing areas  
446 including LGN, SC, and VC (Van Camp et al., 2006), (Christopher P. Pawela et al., 2008). In  
447 addition to these activating regions, we detected deactivating regions that demonstrated reduced  
448 activity during visual stimulation and displayed increased activity during rest i.e. TeA/AC and RC.  
449 Interestingly, these areas have been shown to be nodes of the DMLN in rats (Lu et al., 2012). This  
450 finding seems in contrast to earlier human studies that did not detect significant reductions in DMN  
451 activity during passive sensory processing states that have low cognitive demand e.g. flashing  
452 checkerboard pattern presentation (Greicius et al., 2003). However, a number of important  
453 differences in our study could explain this discrepancy. Firstly, it should be noted that the effect  
454 we found in rats was very subtle. Thus, it is possible that similar effects could be present in humans

455 but not sufficiently strong to be detected during awake conditions that are potentially compromised  
456 by additional processes. Previous studies directly demonstrated that the magnitude and extent of  
457 the suppression depends on the difficulty of the cognitive task (Leech et al., 2011; Mayer et al.,  
458 2010). As our study was performed in anesthetized rats, although not optimal for top-down  
459 cognitive processing, could be beneficial for identifying subtle bottom-up effects that could be  
460 otherwise hindered by additional variability induced by awake conditions. An alternative  
461 explanation is that in rodents passive sensory stimulation is more cognitively demanding in  
462 comparison to humans. Visual stimulation in rodents is thought to increase behavior mechanisms  
463 such as fear, which could be responsible for modulating the DMLN (McClearn, 1960). As previous  
464 studies in human have shown, fear can readily deactivate the DMN (Marstaller et al., 2017). Our  
465 observation could therefore suggest stronger cognitive involvement in rats during visual  
466 stimulation (Anticevic et al., 2013).

#### 467 **4.2. Continuous visual stimulation decreases inter- and intra-network FC of the DMLN**

468 We explored the reorganization of functional networks during a visually stimulated brain state  
469 induced by CVS. The CVS paradigm was specifically developed to get the animal in a visually  
470 attentive stimulated steady state and stochasticity was included to avoid habituation towards the  
471 stimulus. Firstly, ICA analysis was performed on the RSB data in order to identify the RSNs. These  
472 networks showed strong bilateral connectivity and were similar to previously described networks  
473 in rats (Hutchison et al., 2010; Jonckers et al., 2011). We then investigated how the activity and  
474 connectivity within and across these networks changed in the CVS condition.

475 By comparing FC between networks in both conditions, we demonstrated that CVS decreased inter-  
476 network FC between DMLN subcomponents (cingulate-retrosplenial and temporal-prefrontal  
477 networks (Lu et al., 2012)) and with the visual network. The observed decrease in inter-network  
478 connectivity during the CVS condition suggests an alteration in communication between the



479 DMLN and the visual network. This finding could subserve the enhancement of local, input  
480 specific visual processing during CVS versus a higher inter-network communication during rest  
481 conditions.

482 Further, we performed ROI based analysis focusing on areas within the DMLN. This analysis  
483 demonstrated that intra-DMLN FC was also decreased. This included connections between  
484 multiple major nodes of the DMLN *i.e* Cg-RS, Cg-PtA, RS-PtA and RS-TeA. Similar to activity  
485 level decreases, connectivity decreases within human DMN were previously observed only with  
486 tasks involving higher cognitive load (Elton and Gao, 2015; Fransson, 2006; Gao et al., 2013;  
487 Marrelec and Fransson, 2011), while simple visual stimulation with a constantly flickering  
488 checkerboard pattern were not able to induce such deactivation (Di et al., 2015). Interestingly, the  
489 results observed in our study are more consistent with human data from subjects in a higher  
490 attentive and cognitive brain state.

491

## 492 **5. Conclusion**

493 In summary, we demonstrated that simple yet stochastic sensory stimulation in anesthetized rats  
494 could a) deactivate certain nodes of the DMLN, and b) reduce intra- and inter-DMLN network  
495 connectivity simulating similar results in humans performing task involving high cognitive and  
496 top-down attentional demand. We conjecture that the stochasticity of our stimulus, may play an  
497 important role in consistently and continuously driving bottom-up attention triggering mechanisms.  
498 Given that the bottom-up and top-down attentional systems share specific network components  
499 (Katsuki and Constantinidis, 2014), we suggest that both attention mechanisms are able to  
500 deactivate and reduce functional connectivity of the DMN. These results are very significant and  
501 could prove immensely useful not only for our better understanding of the DMN using animal  
502 models but are also very promising for being used in human patients that are anesthetized or non-

503 responsive as a result of trauma and or injury. However, to more explicitly demonstrate the link  
504 between attention systems and DMN activity and connectivity, more studies are required both in  
505 humans using stimuli specifically designed to continuously drive bottom-up attention, as well as in  
506 awake and behaving animals including more complicated cognitive tasks.

### 507 **Acknowledgements**

508 This research was supported by the fund of scientific research Flanders (FWO G048917N),  
509 Flagship ERA-NET (FLAG-ERA) FUSIMICE (grant agreement G.0D7651N) and University  
510 Research Fund of University of Antwerp (BOF DOCPRO FFB150340).

### 511 512 **Reference list**

- 513 Anticevic, A., Cole, M., Murray, J., Corlett, P., Wang, X.-J., Krystal, J., 2013. The Role of Default  
514 Network Deactivation in Cognition and Disease. *Trends Cogn. Sci.* 16, 584–592.  
515 <https://doi.org/10.1016/j.tics.2012.10.008>.The
- 516 Bertero, A., Liska, A., Pagani, M., Parolisi, R., Masferrer, M.E., Gritti, M., Pedrazzoli, M.,  
517 Galbusera, A., Sarica, A., Cerasa, A., Buffelli, A., Tonini, R., Buffo, A., Gross, C., Pasqualetti,  
518 M., Gozzi, A., 2018. Autism-associated 16p11.2 microdeletion impairs prefrontal functional  
519 connectivity in mouse and human. *Brain* 141, 2055–2065.  
520 <https://doi.org/10.1093/brain/awy111>
- 521 Buckner, R.L., Andrews-Hanna, J.R., Schacter, D.L., 2008. The brain’s default network: Anatomy,  
522 function, and relevance to disease. *Ann. N. Y. Acad. Sci.* 1124, 1–38.  
523 <https://doi.org/10.1196/annals.1440.011>
- 524 Calhoun, V.D., Lui, J., Adali, T., 2009. A review of group ICA for fMRI data and ICA for joint  
525 inference of imaging, genetic, and ERP data. *Neuroimage* 45, S163–S172.  
526 <https://doi.org/10.1016/j.neuroimage.2008.10.057>.A

- 527 Damoiseaux, J.S., Rombouts, S.A.R.B., Barkhof, F., Scheltens, P., Stam, C.J., Smith, S.M.,  
528 Beckmann, C.F., 2006. Consistent resting-state networks across healthy subjects. *Proc. Natl.*  
529 *Acad. Sci.* 103, 13848–13853. <https://doi.org/10.1073/pnas.0601417103>
- 530 Di, X., Fu, Z., Chan, S.C., Hung, Y.S., Biswal, B.B., Zhang, Z., 2015. Task-related functional  
531 connectivity dynamics in a block-designed visual experiment. *Front. Hum. Neurosci.* 9, 1–11.  
532 <https://doi.org/10.3389/fnhum.2015.00543>
- 533 Elton, A., Gao, W., 2015. Task-positive Functional Connectivity of the Default Mode Network  
534 Transcends Task Domain. *J. Cogn. Neurosci.* 27, 2369–2381.  
535 [https://doi.org/10.1162/jocn\\_a\\_00859](https://doi.org/10.1162/jocn_a_00859)
- 536 Fox, M.D., Snyder, A.Z., Vincent, J.L., Corbetta, M., Van Essen, D.C., Raichle, M.E., 2005. The  
537 human brain is intrinsically organized into dynamic, anticorrelated functional networks. *Proc.*  
538 *Natl. Acad. Sci.* 102, 9673–9678. <https://doi.org/10.1073/pnas.0504136102>
- 539 Fransson, P., 2006. How default is the default mode of brain function?. Further evidence from  
540 intrinsic BOLD signal fluctuations. *Neuropsychologia* 44, 2836–2845.  
541 <https://doi.org/10.1016/j.neuropsychologia.2006.06.017>
- 542 Friston, K.J., 2011. Functional and Effective Connectivity: A Review. *Brain Connect.* 1, 13–36.  
543 <https://doi.org/10.1089/brain.2011.0008>
- 544 Gao, W., Gilmore, J.H., Alcauter, S., Lin, W., 2013. The dynamic reorganization of the default-  
545 mode network during a visual classification task. *Front. Syst. Neurosci.* 7, 1–13.  
546 <https://doi.org/10.3389/fnsys.2013.00034>
- 547 Gozzi, A., Schwarz, A.J., 2016. Large-scale functional connectivity networks in the rodent brain.  
548 *Neuroimage* 127, 496–509. <https://doi.org/10.1016/j.neuroimage.2015.12.017>
- 549 Greicius, M., 2008. Resting-state functional connectivity in neuropsychiatric disorders. *Curr. Opin.*  
550 *Neurol.* 24, 424–430. <https://doi.org/10.1097/WCO.0b013e328306f2c5>

- 551 Greicius, M.D., Krasnow, B., Reiss, A.L., Menon, V., 2003. Functional connectivity in the resting  
552 brain: a network analysis of the default mode hypothesis. *Proc. Natl. Acad. Sci. U. S. A.* 100,  
553 253–8. <https://doi.org/10.1073/pnas.0135058100>
- 554 Hahn, B., Ross, T.J., Stein, E.A., 2007. Cingulate activation increases dynamically with response  
555 speed under stimulus unpredictability. *Cereb. Cortex* 17, 1664–1671.  
556 <https://doi.org/10.1093/cercor/bhl075>.Cingulate
- 557 Hull, J. V., Jacones, Z.J., Torgerson, C.M., Irimia, A., Van Horn, J.D., Aylward, E., Bernier, R.,  
558 Bookheimer, S., Dapretto, M., Gaab, N., Geschwind, D., Jack, A., Nelson, C., Pelphrey, K.,  
559 State, M., Ventola, P., Webb, S.J., 2017. Resting-state functional connectivity in autism  
560 spectrum disorders: A review. *Front. Psychiatry* 7. <https://doi.org/10.3389/fpsyt.2016.00205>
- 561 Hutchison, R.M., Mirsattari, S.M., Jones, C.K., Gati, J.S., Leung, L.S., 2010. Functional Networks  
562 in the Anesthetized Rat Brain Revealed by Independent Component Analysis of Resting-State  
563 fMRI 3398–3406. <https://doi.org/10.1152/jn.00141.2010>.
- 564 Jonckers, E., Van Auerkerke, J., De Visscher, G., Van der Linden, A., Verhoye, M., 2011.  
565 Functional connectivity fMRI of the rodent brain: comparison of functional connectivity  
566 networks in rat and mouse. *PLoS One* 6, e18876.  
567 <https://doi.org/10.1371/journal.pone.0018876>
- 568 Katsuki, F., Constantinidis, C., 2014. Bottom-up and top-down attention: Different processes and  
569 overlapping neural systems. *Neuroscientist* 20, 509–521.  
570 <https://doi.org/10.1177/1073858413514136>
- 571 Krishnan, G.P., González, O.C., Bazhenov, M., 2018. Origin of slow spontaneous resting-state  
572 neuronal fluctuations in brain networks. *Proc. Natl. Acad. Sci.* 201715841.  
573 <https://doi.org/10.1073/pnas.1715841115>
- 574 Laird, A.R., Eickhoff, S.B., Li, K., Robin, D.A., Glahn, D.C., Fox, P.T., 2009. Investigating the

- 575 Functional Heterogeneity of the Default Mode Network Using Coordinate-Based Meta-  
576 Analytic Modeling. *J. Neurosci.* 29, 14496–14505.  
577 <https://doi.org/10.1523/JNEUROSCI.4004-09.2009>
- 578 Leech, R., Kamourieh, S., Beckmann, C.F., Sharp, D.J., 2011. Fractionating the Default Mode  
579 Network: Distinct Contributions of the Ventral and Dorsal Posterior Cingulate Cortex to  
580 Cognitive Control. *J. Neurosci.* 31, 3217–3224. [https://doi.org/10.1523/JNEUROSCI.5626-](https://doi.org/10.1523/JNEUROSCI.5626-10.2011)  
581 [10.2011](https://doi.org/10.1523/JNEUROSCI.5626-10.2011)
- 582 Li, Q., Li, G., Wu, D., Lu, H., Hou, Z., Ross, C.A., Yang, Y., Zhang, J., Duan, W., 2017. Resting-  
583 state functional MRI reveals altered brain connectivity and its correlation with motor  
584 dysfunction in a mouse model of Huntington’s disease. *Sci. Rep.* 7, 1–9.  
585 <https://doi.org/10.1038/s41598-017-17026-5>
- 586 Lin, P., Yang, Y., Gao, J., De Pisapia, N., Ge, S., Wang, X., Zuo, C.S., Jonathan Levitt, J., Niu, C.,  
587 2017. Dynamic Default Mode Network across Different Brain States. *Sci. Rep.* 7, 1–13.  
588 <https://doi.org/10.1038/srep46088>
- 589 Liska, A., Galbusera, A., Schwarz, A.J., Gozzi, A., 2015. Functional connectivity hubs of the  
590 mouse brain. *Neuroimage* 115, 281–291. <https://doi.org/10.1016/j.neuroimage.2015.04.033>
- 591 Lu, H., Zou, Q., Gu, H., Raichle, M.E., Stein, E.A., Yang, Y., 2012. Rat brains also have a default  
592 mode network. *Proc. Natl. Acad. Sci.* 109, 3979–3984.  
593 <https://doi.org/10.1073/pnas.1200506109>
- 594 Ma, Y., Shaik, M.A., Kozberg, M.G., Kim, S.H., Portes, J.P., Timerman, D., Hillman, E.M.C.,  
595 2016. Resting-state hemodynamics are spatiotemporally coupled to synchronized and  
596 symmetric neural activity in excitatory neurons. *Proc. Natl. Acad. Sci.* 113, E8463–E8471.  
597 <https://doi.org/10.1073/pnas.1525369113>
- 598 Marrelec, G., Fransson, P., 2011. Assessing the influence of different ROI Selection Strategies on

599 functional connectivity analyses of fMRI Data acquired during steady-state conditions. PLoS  
600 One 6, 1–14. <https://doi.org/10.1371/journal.pone.0014788>

601 Marstaller, L., Burianová, H., Reutens, D.C., 2017. Adaptive contextualization: A new role for the  
602 default mode network in affective learning. *Hum. Brain Mapp.* 38, 1082–1091.  
603 <https://doi.org/10.1002/hbm.23442>

604 Mayer, J.S., Roebroeck, A., Maurer, K., Linden, D.E.J., 2010. Specialization in the default mode:  
605 Task-induced brain deactivations dissociate between visual working memory and attention.  
606 *Hum. Brain Mapp.* 31, 126–139. <https://doi.org/10.1002/hbm.20850>

607 McClearn, G.E., 1960. Strain differences in activity of mice: Influence of illumination. *J. Comp.*  
608 *Physiol. Psychol.* 53, 142–143. <https://doi.org/10.1037/h0042766>

609 Nestler, E.J., Hyman, S.E., 2010. Animal models of neuropsychiatric disorders. *Nat. Neurosci.* 13,  
610 1161–1169. <https://doi.org/10.1038/nn.2647>

611 Pan, W.-J., Billings, J.C.W., Grooms, J.K., Shakil, S., Keilholz, S.D., 2015. Considerations for  
612 resting state functional MRI and functional connectivity studies in rodents. *Front. Neurosci.*  
613 9, 20130152. <https://doi.org/10.3389/fnins.2015.00269>

614 Pawela, C.P., Biswal, B.B., Cho, Y.R., Kao, D.S., Li, R., Jones, S.R., Schulte, M.L., Matloub, H.S.,  
615 Hudetz, A.G., Hyde, J.S., 2008. Resting-state functional connectivity of the rat brain. *Magn.*  
616 *Reson. Med.* 59, 1021–1029. <https://doi.org/10.1002/mrm.21524>. Resting-State

617 Pawela, C.P., Hudetz, A.G., Ward, D.B., Schulte, M.L., Li, R., Kao, D.S., Mauck, M.C., Cho, Y.R.,  
618 Neitz, J., James, H.S., 2008. Modeling of region-specific fMRI BOLD neurovascular response  
619 functions in rat brain reveals residual differences that correlate with the differences in regional  
620 evoked potentials 41, 525–534. <https://doi.org/10.1016/j.neuroimage.2008.02.022>. Modeling

621 Petridou, N., Gaudes, C.C., Dryden, I.L., Francis, S.T., Gowland, P.A., 2013. Periods of rest in  
622 fMRI contain individual spontaneous events which are related to slowly fluctuating

623 spontaneous activity. *Hum. Brain Mapp.* 34, 1319–1329. <https://doi.org/10.1002/hbm.21513>

624 Rohleder, C., Wiedermann, D., Neumaier, B., Drzezga, A., Timmermann, L., Graf, R., Leweke,  
625 F.M., Endepols, H., 2016. The Functional Networks of Prepulse Inhibition: Neuronal  
626 Connectivity Analysis Based on FDG-PET in Awake and Unrestrained Rats. *Front. Behav.*  
627 *Neurosci.* 10, 1–10. <https://doi.org/10.3389/fnbeh.2016.00148>

628 Salvador, R., Suckling, J., Coleman, M.R., Pickard, J.D., Menon, D., Bullmore, E., 2005.  
629 Neurophysiological architecture of functional magnetic resonance images of human brain.  
630 *Cereb. Cortex* 15, 1332–2342. <https://doi.org/10.1093/cercor/bhi016>

631 Schwarz, A.J., Gass, N., Sartorius, A., Risterucci, C., Spedding, M., Schenker, E., Meyer-  
632 Lindenberg, A., Weber-Fahr, W., 2013. Anti-Correlated Cortical Networks of Intrinsic  
633 Connectivity in the Rat Brain. *Brain Connect.* 3, 503–511.  
634 <https://doi.org/10.1089/brain.2013.0168>

635 Shah, D., Jonckers, E., Praet, J., Vanhoutte, G., Delgado Y Palacios, R., Bigot, C., D’Souza, D. V,  
636 Verhoye, M., Van der Linden, A., 2013. Resting state fMRI reveals diminished functional  
637 connectivity in a mouse model of amyloidosis. *PLoS One* 8, e84241.  
638 <https://doi.org/10.1371/journal.pone.0084241>

639 Shah, D., Praet, J., Latif Hernandez, A., Höfling, C., Anckaerts, C., Bard, F., Morawski, M., Detrez,  
640 J.R., Prinsen, E., Villa, A., De Vos, W.H., Maggi, A., D’Hooge, R., Balschun, D., Rossner,  
641 S., Verhoye, M., Van der Linden, A., 2016. Early pathologic amyloid induces hypersynchrony  
642 of BOLD resting-state networks in transgenic mice and provides an early therapeutic window  
643 before amyloid plaque deposition. *Alzheimer’s Dement.* 12, 964–976.  
644 <https://doi.org/10.1016/j.jalz.2016.03.010>

645 Sierakowiak, A., Monnot, C., Aski, S.N., Uppman, M., Li, T.Q., Damberg, P., Brené, S., 2015.  
646 Default mode network, motor network, dorsal and ventral basal ganglia networks in the rat

647 brain: Comparison to human networks using resting state-fMRI. *PLoS One* 10, 1–20.  
648 <https://doi.org/10.1371/journal.pone.0120345>

649 Stafford, J.M., Jarrett, B.R., Miranda-Dominguez, O., Mills, B.D., Cain, N., Mihalas, S., Lahvis,  
650 G.P., Lattal, K.M., Mitchell, S.H., David, S. V, Fryer, J.D., Nigg, J.T., Fair, D.A., 2014. Large-  
651 scale topology and the default mode network in the mouse connectome. *Proc. Natl. Acad. Sci.*  
652 111, 18745–18750. <https://doi.org/10.1073/pnas.1404346111>

653 Trancikova, A., Ramonet, D., Moore, D.J., 2011. Genetic mouse models of neurodegenerative  
654 diseases, 1st ed, *Progress in Molecular Biology and Translational Science*. Elsevier Inc.  
655 <https://doi.org/10.1016/B978-0-12-384878-9.00012-1>

656 Van Camp, N., Verhoye, M., De Zeeuw, C.L., Van der Linden, A., 2006. Light Stimulus Frequency  
657 Dependence of Activity in the Rat Visual System as Studied With High-Resolution BOLD  
658 fMRI. *J. Neurophysiol.* 95, 3164–3170. <https://doi.org/10.1152/jn.00400.2005>

659 van den Heuvel, M.P., Hulshoff Pol, H.E., 2010. Exploring the brain network: A review on resting-  
660 state fMRI functional connectivity. *Eur. Neuropsychopharmacol.* 20, 519–534.  
661 <https://doi.org/10.1016/j.euroneuro.2010.03.008>

662 Zhou, J., Liu, S., Ng, K.K., Wang, J., 2017. Applications of Resting-State Functional Connectivity  
663 to Neurodegenerative Disease. *Neuroimaging Clin. N. Am.* 27, 663–683.  
664 <https://doi.org/10.1016/j.nic.2017.06.007>

665

666